Digest Journal of Nanomaterials and Biostructures Vol. 19, No. 3, July -September 2024, p. 1265 - 1276

Advancing PV technology with ZnO/Ag+ nanocomposites

V. Revathi[a], S. Sheeba Rani[b], M. Balamurugan[c], T. Manikumar[d], S. Sivakumar[e,*], B. Sangeetha[f]

[a]*Department of R&D, New Horizon College of Engineering, Bengaluru, India*
[b]*Department of* Electronics and Communication Engineering*, Sri Eshwar College of Engineering, Coimbatore.*
[c]*Centre for Photonics and Nanotechnology, Department of Chemistry, Sona College of Technology, Salem, Tamilnadu, India*
[d]*Department of computer science and Engineering, Kalasalingam Academy of Research and Education, (Deemed to be University), Krishnan Kovil, Tamilnadu, India*
[e]*Department of Physics, Government Arts College (Autonomous), Salem, Tamilnadu, India*
[f] *Department of Electrical and Electronics Engineering, AVS Engineering College, Salem, Tamilnadu, India*

This study focuses on the synthesis and characterization of hybrid zinc oxide/silver ion (ZnO/Ag+) nanocomposites tailored for PV cell applications. The nanocomposites are synthesized through a cost-effective method, leveraging the unique properties of both ZnO and Ag. Characterization techniques including X-ray diffraction (XRD), scanning electron microscopy (SEM) are employed to analyze the structural, morphological and optical properties of the nanocomposites. Moreover, the electrical properties and photoelectric performance of the PV solar cells are evaluated and compared with conventional PV devices. The results demonstrate the potential of ZnO/Ag+ nanocomposites in enhancing the overall performance of PV solar cells.

(Received June 3, 2024; Accepted August 29, 2024)

Keywords: Sol-gel synthesis, Ag, ZnO, PV applications, XPS, SEM

1. Introduction

Zinc oxide (ZnO) holds significant importance in industry due to its inorganic and semiconducting nature, characterized by inherent properties aligned with the wurtzite structure [1]. The optical features of ZnO nanocomposites have generated interest, as these particles exhibit transparency to visible light while absorbing UV-light. Intensive research has been devoted to exploring ZnO's unique properties, leading to its applications in chemical sensors etc., [2–8]. Metal nanoparticles, particularly silver, have captivated scientific attention for their distinctive properties, contributing to advancements in electronics, materials science, and medicine [9-10]. Silver nanoparticles find applications in various fields such as optical receptors, bio labeling, etc.,. This work focuses on silver (Ag) as a doping agent with ZnO. The straightforward link matrices of Ag ions make their behavior crucial in nanomaterials, especially as the size diminishes. The sol-gel synthesis method is widely employed for generating novel nanomaterials with distinct properties. This method is particularly advantageous in producing ZnO-Ag nanocomposites, as it facilitates the formation of nanorods of smaller size compared to other reported methods [11-13]. The chemical precipitation method through sol gel process offers several benefits. Hence, this work synthesized ZnO-Ag nanocomposites by sol-gel method. The synthesized ZnO nanoparticles underwent comprehensive characterization through structural, optical, and morphological studies and its application towards Solar cells is analysed.

* Corresponding author: sivaphotonics@gmail.com
https://doi.org/10.15251/DJNB.2024.193.1265

2. Materials and methods

Analytical-grade chemicals, including zinc acetate dihydrate, silver nitrate, sodium hydroxide, and ethanol, were procured and utilized without further purification. A solution was prepared by combining 1M zinc chloride ($ZnCl_2$) and 1M silver nitrate ($AgNO_3$) with 1M sodium hydroxide (NaOH) in 100mL of distilled water. The resulting dense suspensions underwent centrifugation at 5000 rpm for 30 minutes, and the supernatant was removed through decantation. The obtained materials underwent aging at room temperature, followed by two washes with absolute ethanol. Following each washing step, the solvent was isolated through centrifugation. The gathered material underwent air-drying overnight, followed by grinding into a fine powder. These powders were then subjected to calcination at 400°C, leading to the formation of ZnO-Ag nanocomposites.

3. Characterization analysis

The structure of the ZnO-Ag nanocomposites prepared was analyzed using X-ray diffraction (XRD) patterns. Optical properties were studied using UV-VIS spectrophotometer. The chemical compositions were examined by X-ray photoelectron spectroscopy (XPS). Finally, the Auger parameters were determined by measuring them with monochromatic X-ray of Al Kα ($h\nu$ = 1486.6 eV).

3.1 Structural analysis

The XRD patterns of this nanocomposite reveals a wurtzite hexagonal phase, as depicted in Figure 1. The figure illustrates XRD peaks corresponding to specific crystallographic planes. The peaks at 2θ values (38.10°, 44.28°, and 64.45°) associated with the planes (111, 200 220), indicate the presence of Ag and belong to the face-centered-cubic (FCC) structure (JCPDS no. 89-3722).

ZnO exhibits a wurtzite structure, characterized by hexagonal closed packing of oxygen atoms with zinc atoms occupying half of the tetrahedral sites. Upon doping with Ag in the ZnO structure, the appearance of Ag peaks at angles (38.10°, 44.28°, and 64.45°) in ZnO-Ag confirms the presence of the Ag phase within the ZnO matrix. Notably, the doping induces subtle changes without altering the overall material structure.

To gain further insights, various parameters were calculated to understand the mechanical stress resulting from the injection of impurities. The size difference in ionic radii, stemming from the substitution of Zn^{2+} with smaller ions, causes this stress. Silver, with ionic radii in different valence states (Ag^{3+}, Ag^{2+}, and Ag^{1+}), may replace Zn^{2+} ions. Depending on the valence state and disparities in ionic radii, Ag and Zn, the replacement either expands or narrows lattice parameters [14].

The results affirm that the nanocomposite products consist of pure phases. Additionally, the narrower XRD diffraction peaks indicates a well-defined crystalline nature of Ag: ZnO nanocomposites, with no discernible peaks from impurities. This indicates that the deposition of silver has no effect on the crystalline properties of the ZnO structure.

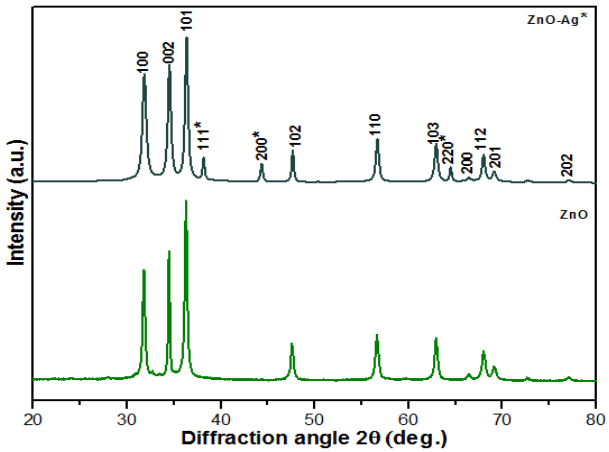

Fig. 1. XRD patterns of ZnO-Ag nanocomposites.

The crystallite size of ZnO-Ag nanocomposites, determined using Scherrer's formula and presented in Table 1, ranges from 16 to 38 nm. As the crystallite size increases, stacking faults, dislocation density and elastic strains decrease accordingly. This indicates that the ZnO-Ag nanocomposites possess high crystalline quality, along with reduced elastic strains. These findings suggest that the sol-gel method is effective for synthesizing high-quality, polycrystalline ZnO-Ag nanocomposites.

Table 1. Structural parameters of ZnO-Ag nanocomposites.

Planes	**Size of the Crystallite (D-nm)**	**Dislocation Density - δ (10^{15} lines / m^2)**	**Probability of Stacking faults (Å)**	**Elastic strains (Ɛ)**
100	16.60	3.6306	0.0080	0.0043
002	21.49	2.1661	0.0057	0.0032
101	25.20	1.5753	0.0046	0.0027
111*	38.00	0.6927	0.0029	0.0017
200*	31.02	1.0393	0.0031	0.0020
102*	31.40	1.0142	0.0029	0.0019

3.2. UV-visible absorption analysis

The UV-Vis absorption spectra, depicted in Figure 2, were meticulously recorded for the ZnO-Ag nanocomposite material under room temperature conditions. A distinctive plasmonic resonance peak emerges at 310 nm [15-16] within the UV-Vis spectra. This resonance is a consequence of an augmented presence of Ag particles dispersed throughout the ZnO matrix, effectively enhancing the nanocomposite's surface area. The observable plasmonic resonance peak is a crucial indicator of the interaction and distribution of metallic components on the nanocomposite surface.

The method employed in presenting and elevating ZnO-Ag composite nanorods through UV absorption holds notable importance. The heightened absorbance, particularly in the UV range, underscores the efficiency of this nanocomposite for various industrial applications, where optical properties play a pivotal role. The determination of band gap values for the ZnO-Ag nanocomposite is conducted through Tauc plot analysis. This analytical approach provides valuable insights into the energy levels and electronic transitions occurring within the nanocomposite, further contributing to a comprehensive understanding of its optical properties. The following equation expresses the relationship between the absorption coefficient (α) and the incident photon energy (hν).

$$(\alpha h\nu) = A(h\nu - E_g)^n$$

where, A - constant, E_g - bandgap of the material

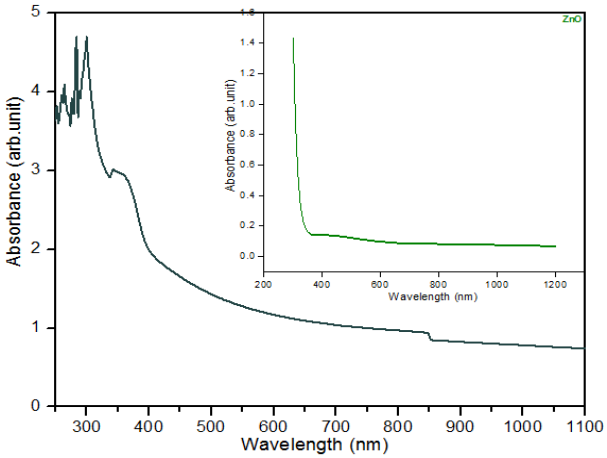

Fig. 2. Optical absorbance spectra of ZnO-Ag nanocomposites.

Tauc plots have been shown in Figure.3. The investigation of the bandgap in ZnO-Ag nanocomposites was conducted through UV-Vis spectra within the range of 200–1100 nm. The determined bandgap energy values for ZnO-Ag nanocomposites reveal a reduction in exciton absorptions, decreasing from 3.5 eV to 2.45 eV with the incorporation of silver content into ZnO nanoparticles. The absorption spectra clearly exhibits the strong interaction between ZnO and silver oxide.

The optical measurements of this nanostructures demonstrate a robust red shift, underscoring the pronounced interaction between Ag-ion's d-element and the host zinc oxide's s- and p-electrons. The interchange of sp-d and p-d band electrons induces a renormalization effect, leading to corrections in the valence bandgap and conduction band edges, ultimately resulting in a reduced bandgap.

The absence of a surface plasmon resonance (SPR) peak in the range of 400 to 850 nm states about the coupling between Ag and ZnO. Thus, a notable decrease in the bandgap energy, 2.45 eV lower than that of pure ZnO nanoparticles, is detected in the ZnO-Ag nanocomposites. This decrease in bandgap energy facilitates easy electron transport from valence to conduction band. Thus, the enhanced absorption of nanoparticles, resulting from Ag doping, holds significant potential for a wide range of PV applications [17–18].

3.3. XPS analysis

XPS analysis were accomplished to investigate the chemical composition of the materials. Figure 4 illustrates photoelectron peaks ranging from 0 to 1100 eV for most naturally occurring elements. Clear and distinct peaks corresponding to Zn, O, and Ag are prominent in the graphs. Symmetrical peaks at 1044.32 and 1026.25 eV for ZnO-Ag nanocomposites are attributed to Zn ($2p_{1/2}$) and Zn($2p_{3/2}$). The observed splitting of Zn 2p states by approximately 18.07 eV is a result of powerful spin-orbit coupling [11]. These peaks confirm the presence of the wurtzite structure and Zn^{2+} mode of Zn atoms. However, the binding energy of Zn in ZnO-Ag nanocomposites has decreased from the pure ZnO value of 24 eV to 18.07 eV, indicating that the introduction of the doping element Ag has diminished the electron binding affinity.

The Ag ($3p_{1/2}$) and Ag ($3p_{3/2}$) peaks (at 602.37 and 572.37 eV) depicts a split of approximately ~30 eV, indicates the metallic state of silver. The relation between Ag and ZnO nanoparticles plays a role in regulating the Fermi levels of Ag and ZnO. Owing to the increased electronegativity of Ag, an electron transfer from Zn to Ag particles is assumed to occur, highlighting silver's influence over controlling defects within the ZnO crystal lattice. The presence

of Auger lines in the complex patterns of the LMM groups further enhances the understanding of the XPS patterns.

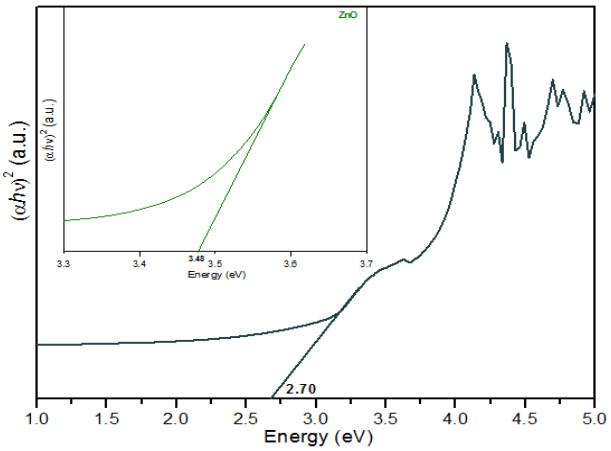

Fig. 3. Optical bandgap of ZnO-Ag nanocomposites.

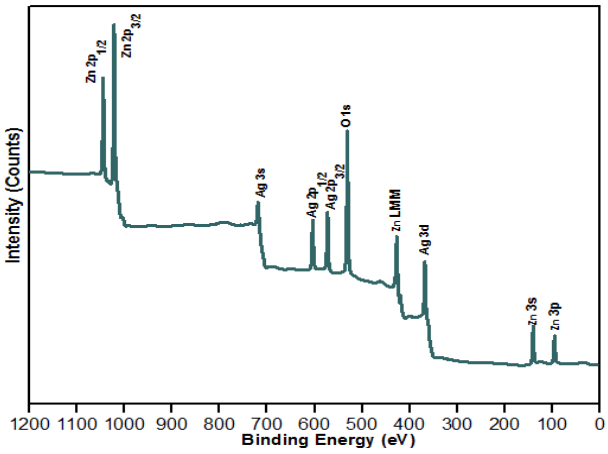

Fig. 4. XPS analysis of ZnO-Ag nanocomposites.

3.4. Vibrating sample magnetometry (VSM) measurements

Figure 5 illustrates the magnetic characterization of ZnO-Ag nanocomposites at room temperature, revealing their ferromagnetic ordering. The figure shows that pure ZnO exhibits weak ferromagnetic behavior at room temperature, which is significantly enhanced when ZnO is doped with Ag. The weak diamagnetic nature observed in undoped ZnO nanoparticles is likely due to the formation of voids during their preparation, with contributions from both oxygen and zinc.

The ferromagnetism observed in ZnO-Ag nanocomposites arises from both intrinsic and extrinsic factors. XRD and EDS analyses confirm the presence of a single phase in the ZnO-Ag nanocomposites, with no impurities detected. VSM results indicate that when Ag is doped into the ZnO matrix, Ag+ ions replace Zn2+ ions, thereby inducing magnetism in the samples. The magnetism in the material is recognized to the exchange interaction between locally spin polarized electrons and the conductive electrons accompanying with Ag+ ions. This interaction aligns the spins of the Ag+ ions in the same direction, leading to ferromagnetism. The presence of Ag ions in random orientations and the coupling with oxygen voids generate a large number of carriers, which contribute to the random motion of the magnetic moment. The intersections with magnetic

moments align in the same direction as the polarons. Due to the numerous oxygen vacancies, the polarons overlap, resulting in ferromagnetism.

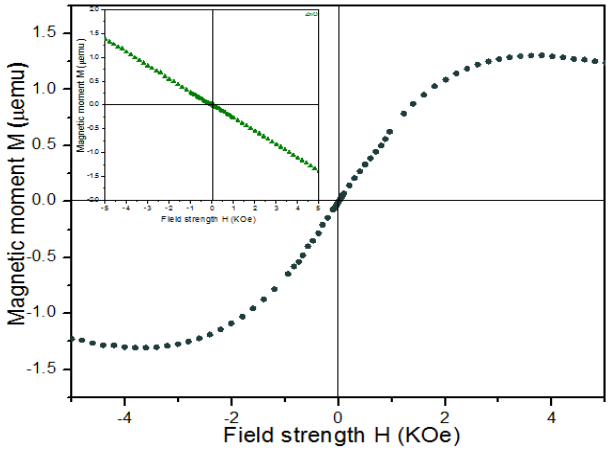

Fig. 5. M–H curves - ZnO-Ag.

3.5. Raman spectra

To explore the effect of Ag doping on the ZnO nanoparticles, Raman spectra were scaled at room temperature. ZnO, known for its wurtzite structure, reveals 8 distinct optical phonon modes at the center of the Brillouin zone, known as the Γ point.

$$\Gamma = 1A_1 + 2B_1 + 1E_1 + 2E_2$$

where A_1 and E_1 - polar branches.

Due to the large electric field linked to longitudinal optical (LO) phonons, these polar branches split into two parts namely, the longitudinal (LO) and transversal optical (TO) components. Similarly, the non-polar E2 mode has two parts, E2L and E2H. The low-frequency (E2L) mode is related to the heavy zinc sublattice, while the high-frequency (E2H) mode is related to oxygen atoms. The modes (A1, E1, E2) appear in both Raman and IR spectra. However, the B1 mode is not active and is called a silent mode. Figure 6 shows the Raman spectrum of ZnO-Ag in the range of 100-1000 cm^{-1}.

In the spectral range of 378 cm^{-1} to 657 cm^{-1}, the A1's TO and LO branches are observed. Generally, the A1 [LO] phonon mode is associated with oxygen vacancies and zinc interstitials in ZnO. The peak at 391 cm^{-1} represents E2H mode of the ZnO hexagonal wurtzite structure and the peak at 343 cm^{-1} is represents the 2nd order Raman spectrum from the zone boundary phonons, specifically 3E2H - E2L. A peak at 564 cm^{-1} is due to the E1 (LO) mode and represents the oxygen deficiency in Ag-doped samples. A unique peak at 461 cm^{-1} is designated as the interstitial surface phonon mode. The Raman peak at 695 cm^{-1} may be referred to the 2nd order phonon mode 2A1[TO]. Thus, it is observed that the intensity of these peaks increases with higher Ag content. Additionally, the peaks at 127 cm^{-1} and 144 cm^{-1} are assigned to the E2L and 2E2L 2nd order phonon modes respectively.

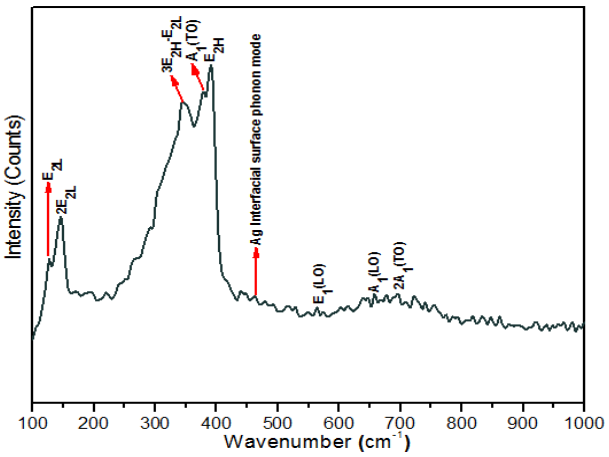

Fig. 6. Raman spectrum - ZnO-Ag.

3.6. SEM analysis

In Figure 7a, scanning electron micrograph illustrates the spherical morphology of the ZnO nanocomposites, which is attributed to the integration of Ag into the ZnO matrix. The SEM images also depict a uniform dispersion of particles throughout the sample.Using image processing tools, a significant investigation into the dimensions of the pores and porosity has been conducted. The particles are homogeneous in shape [19].

Fig. 7b displays the depth map achieved through multilevel thresholding. Fig. 7c accentuates the dark regions, while Fig. 3d repersents the segmented porous areas present within the ZnO sample. Lastly, Fig. 3e presents the distribution of pore sizes.

The porosity percentage, average pore size and standard deviation of pore dimensions are found to be 0.2180%, 2.0603 nm, and 1.2096 nm. Compared to ZnO synthesized using the precursor $ZnCl_2$, which has a porosity of 0.2754%, the addition of Ag to the ZnO matrix results in a decrease in porosity to 0.2180%. While incorporating a dopant into the ZnO semiconductor modifies its structural characteristics, often resulting in a decrease in size. Normally, as particle size increases, porosity diminishes due to chemical aggregation on the finer-textured surface during synthesis. This decline in porosity results in densely packed sediments and reduced permeability. This suggests they are mesoporous materials, suitable for the dye-sensitized solar cell production.

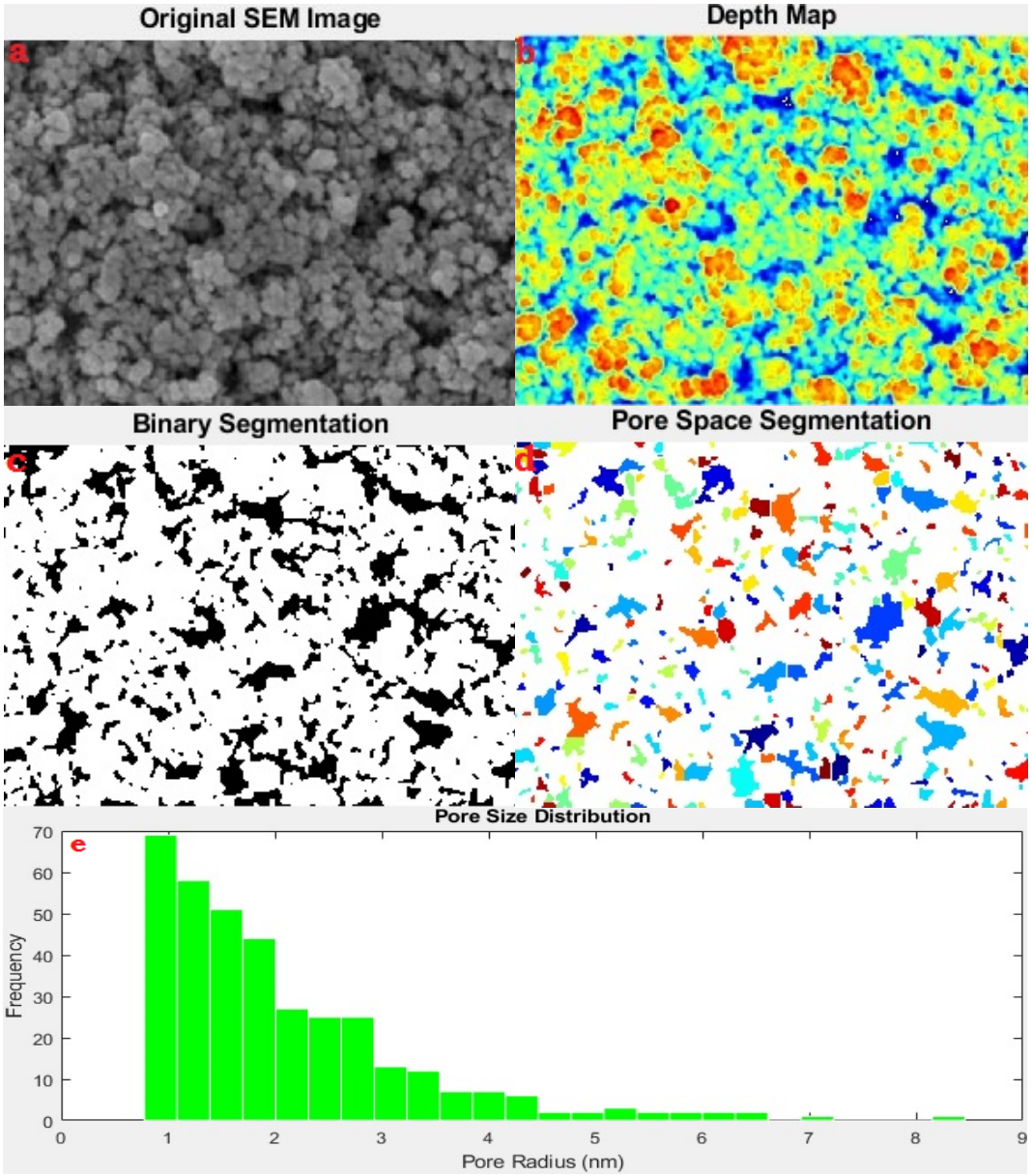

Fig. 7 SEM micrographs-ZnO-Ag.

Figure 8 illustrates the 3D surface roughness of ZnO-Ag nanocomposites, derived from SEM images. Observations indicate that the nanocomposite exhibits lower surface roughness compared to ZnO prepared using zinc chloride. This surface becomes smoother because the nanocomposite has fewer pores. This shows that smoother surfaces have fewer pores.

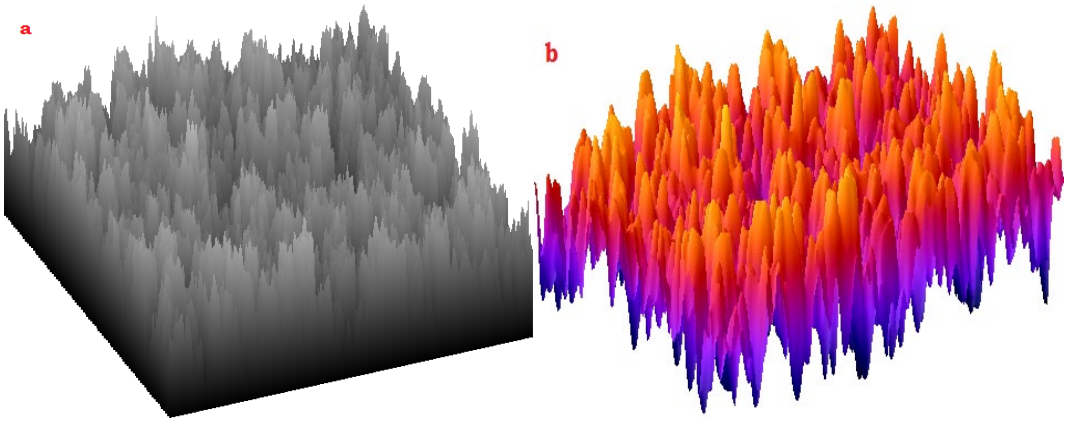

Fig. 8. Surface roughness of ZnO-Ag.

3.7. EDS analysis

Fig. 9 presents the EDS spectra obtained during SEM imaging. Peaks centered around 1.1 keV are associated with the Zn lines, while peaks at 8.6 and 9.7 keV, with fewer counts, are attributed to the Zn Ka and Zn Kb lines, respectively. Peaks around 0.55 keV correspond to the O Ka lines. Similarly, The peaks at 2.9 keV are from the Ag La1 lines, and the peaks at 3.1 keV are due to the Ag Lb1 lines. This is because discrete X-ray quanta from the electron orbital energy levels 3d6 to 2p4 (M5 to L3) produce the Ag La1 line at 2.9 keV and from 3d4 to 2p2 (M4 to L2) produce the Lb1 line. The inset image reveals the EDS of ZnO, revealing that the nanoparticles predominantly contain zinc, silver and oxygen elements.

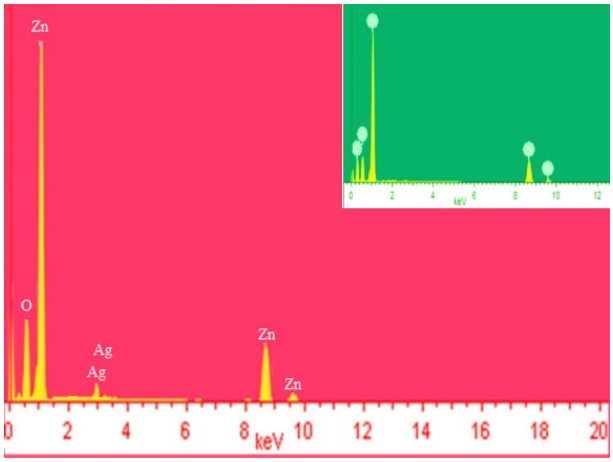

Fig. 9. EDS of ZnO-Ag nanocomposites.

3.8. HRTEM analysis

Figure 10a presents the HRTEM image of the ZnO-Ag nanocomposites, revealing their hexagonal wurtzite structure characterized by the presence of hexagonal facets and spherical structures measuring between 16-38nm. Decorating these structures are smaller particles. To precisely determine the crystal lattice spacing Inverse Fast Fourier Transform (IFFT) and Fast Fourier Transform (FFT) were employed (Fig. 10b). These techniques confirmed a d-spacing value of 0.282 nm for the (100) plane, closely matching standard values. Furthermore, the defects like stacking faults and dislocations is identified from the FFT Sobel filter and is illustrated in Fig. 10c. According to Fig. 10d, the clusters (bluish green lines) denotes the presence of above said defects.

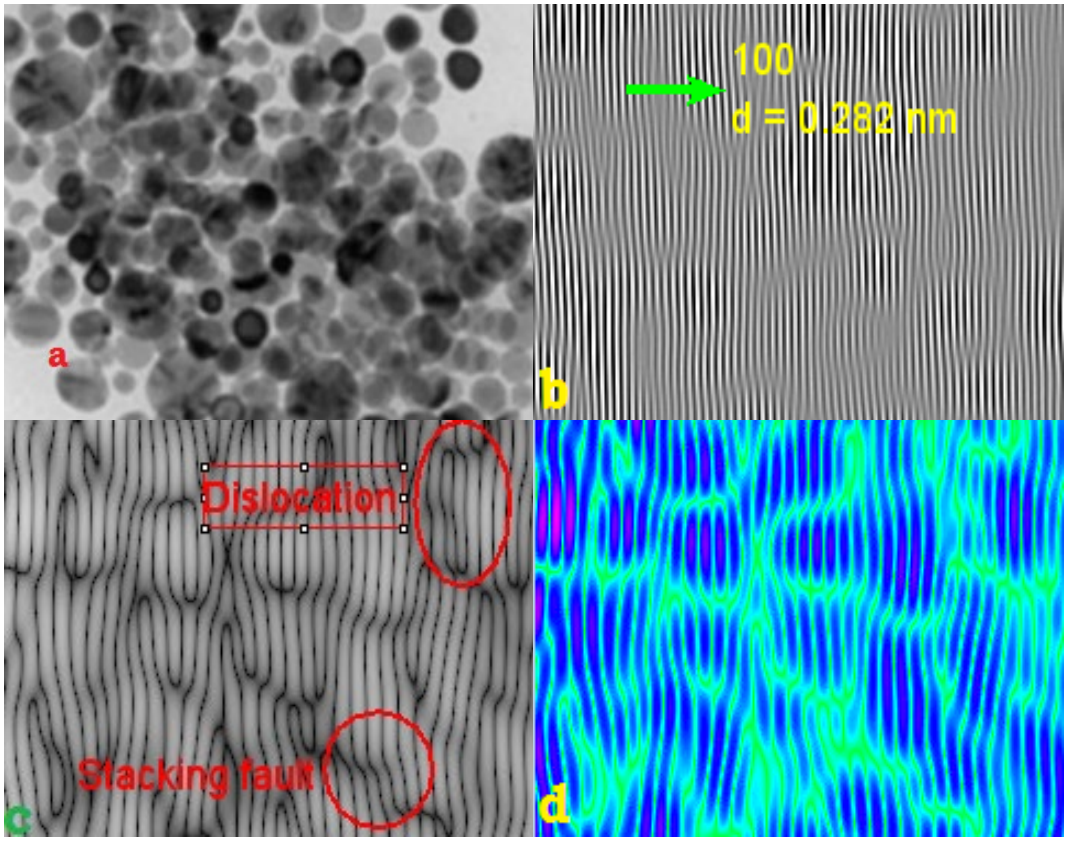

Fig. 10. HRTEM micrographs - ZnO-Ag.

3.9. Photovoltaic performance

A summary of their photovoltaic characterization Dye-Sensitized Solar Cells (DSSCs) employing Ag doped ZnO blended with P3HT is provided in Table 2. From the analysis, it can be found that the DSSC with 7 mol% ZnO-Ag photoanode exhibited remarkable efficiency (η) about 1%, which is the higher than DSSCs fabricated with 7 mol% ZnO-Ag photoanode.

Table 2. Comparison of characteristics of solar cells.

Sample	**I_{SC} (mA/cm^2)**	**V_{OC} (V)**	**Efficiency (η%)**
P3HT-Ag-ZnO (5×10^{-3})	2.34	0.421	0.44
P3HT-Ag-ZnO (7×10^{-3})	6.78	0.403	1

The decrease in the energy gap resulted in enhanced efficiency in utilizing this material within DSSC devices [20,21].

4. Conclusion

The ZnO-Ag nanocomposites prepared by means of sol-gel method can be utilized as a photoanode in PV cells. It can be clearly visualized using various performance measures. XRD analysis affirms the crystalline structure of the composite, highlighting that the introduction of silver does not disrupt the crystalline integrity of the ZnO framework. The bandgap energy of ZnO-Ag nanocomposites demonstrates a reduction in exciton absorptions from 3.5 eV to 2.45 eV. This shift signifies a notable increase in wavelength (a redshift) in the observed absorption spectra, indicating a robust interaction between zinc oxide and silver oxides. XPS analyses reveal distinct peaks corresponding to zinc, oxygen, and silver in the spectra of the synthesized composites. The enhanced absorption of nanoparticles, resulting from Ag doping, holds significant potential for a wide range of PV cells application.

References

[1] Y.K.Mishra, V. S. K. Chakravadhanula, V. Hrkac, Journal of Applied Physics, 112, Article ID064308, 2012; https://doi.org/10.1063/1.4752469

[2] K. Nomura, H. Ohta, K. Ueda, T. Kamiya, M. Hirano, H. Hosono, Science, 300(5623),2003, 1269-1272; https://doi.org/10.1126/science.1083212

[3] S.Y. Lee, E. S. Shim, H. S.Kang, S. S. Pang, J. S.Kang, Thin Solid Films, 473(1), 2005, 31-34; https://doi.org/10.1016/j.tsf.2004.06.194

[4] R. Konenkamp, R. C.Word, C. Schlegel, Applied Physics Letters, 85(24), 2004, 6004-6006; https://doi.org/10.1063/1.1836873

[5] Z. L. Wang, X. Y. Kong, Y. Ding, Advanced Functional Materials, 14(10), 2004, 943-956; https://doi.org/10.1002/adfm.200400180

[6] Y. Ushio, M. Miyayama, H. Yanagida, Sensors and Actuators B, 17(3), 1994, 221- 226; https://doi.org/10.1016/0925-4005(93)00878-3

[7] H. Harima, Journal of Physics Condensed Matter, 16(48), 2004, S5653-S5660; https://doi.org/10.1088/0953-8984/16/48/023

[8] S. J. Pearton, W. H. Heo, M. Ivill, D. P. Norton, T. Steiner, Semiconductor Science and Technology, 19(10), 2004, R59-R74; https://doi.org/10.1088/0268-1242/19/10/R01

[9] M. Ahmad, J. Zhu, J. Mater. Chem. 21, 2011, 599-614; https://doi.org/10.1039/C0JM01645D

[10] S.J. Pearton, D.P. Norton, K. Ip, Y.W. Heo, T. Steiner, Prog. Mater Sci. 50, 2005, 293-340; https://doi.org/10.1016/j.pmatsci.2004.04.001

[11] O. Lupan, L. Chow, L. K.Ono, Journal of Physical Chemistry C, 114(29), 2010, 12401-12408; https://doi.org/10.1021/jp910263n

[12] C. X.Mei, J. Yong, G. X. Yong, Z. X. Wei, Chinese Physics B, 11(21), Article ID 116801, 2012.

[13] M. Mahanti, D. Basak, AIP Conference Proceedings, 1447, 2011, 713-714.

[14] J. El Ghoul, C. Barthou, L. El Mir, Superlattice Microst., 51, 2012, 942-951; https://doi.org/10.1016/j.spmi.2012.03.013

[15] H. Karami, E. Fakoori, Journal of Nanomaterials, 2011, Article ID 628203, 2011, 11; https://doi.org/10.1155/2011/628203

[16] Y.Ni, X. Cao, G. Wu,G.Hu, Z. Yang, X. Wei, Nanotechnology, 18(15), Article ID 155603, 2007; https://doi.org/10.1088/0957-4484/18/15/155603

[17] U.T. Nakate, P. Patil, S.P. Choudhury, S.N. Kale, Nano-Structures & Nano-Objects, 14, 2018, 66-72; https://doi.org/10.1016/j.nanoso.2018.01.007

[18] A. Gupta, Y.N. Lakshmi, R. Manivannan, S.N. Victoria, J. Chil. Chem. Soc. 62, 2017, 3393; https://doi.org/10.4067/S0717-97072017000100018

[19] Sridevi, K.P., Revathi, V., Sangeetha, P., Manjunatha, B. Sivakumar, S., 2024, Digest Journal

of Nanomaterials & Biostructures (DJNB), 19(1); https://doi.org/10.15251/DJNB.2024.191.263
[20] Pushpalatha N., Palpandian P., Banu G., Thirunavukkarasu S., Kokilavani T., Devi B.P., 2023 2023 10th IEEE Uttar Pradesh Section International Conference on Electrical, Electronics and Computer Engineering, UPCON 2023; https://doi.org/10.1109/UPCON59197.2023.10434379.
[21]Anbarasu P., Suresh Kumar R., 2023, Progress in Photovoltaics: Research and Applications, 31(7); https://doi.org/10.1002/pip.3681